Geomechanics and Engineering, *Vol. 43, No. 4 (2025) 329-342*
https://doi.org/10.12989/gae.2025.43.4.329

Effect of low cohesion in sandy soils on seepage-induced failure of circular sheeted excavation pits

Ozan Subasi*

Department of Civil Engineering, Turkish-German University, Istanbul 34820, Turkey

(*Received August 11, 2025, Revised November 4, 2025, Accepted November 5, 2025*)

Abstract. Seepage induced failure mechanisms such as base heave and piping pose serious challenges for the stability of excavation pits in sandy soils. Conventional design approaches rely on Terzaghi's failure criterion and assume fully cohesionless behavior, yet field evidence indicates that even trace cohesion arising from fines content, partial saturation or chemical bonding can meaningfully alter seepage response. To address this gap, the present study employs hydraulically and mechanically coupled axisymmetric finite element analyses to quantify the influence of low cohesion on heave behavior of circular sheeted pits. A homogeneous sand layer is modeled with cohesion values ranging from 0 to 5 kPa, internal friction angles between 25 degrees and 35 degrees and a range of dilation angles. Model results are systematically benchmarked against classical theoretical predictions and reveal three distinct failure modes governed by the interaction of cohesion, friction angle and dilation angle. Results demonstrate that the inclusion of even very low cohesion markedly raises the critical hydraulic gradient required to initiate failure and thereby enhances pit stability. This work offers novel insight by highlighting the importance of incorporating slight cohesion and realistic dilation behavior into seepage stability assessments for deep excavations and other key geotechnical structures.

Keywords: cohesion; finite element; numerical analysis; seepage failure; Terzaghi failure criteria

1. Introduction

In geotechnical engineering, the design and construction of excavation and foundation systems demand a thorough understanding of soil behavior under varying loads and groundwater conditions. A substantial body of research has focused on advancing the understanding of excavation and foundation system design in these challenging conditions, reflecting the breadth of research devoted to improving safety and performance in practice (Sarvesh *et al.* 2023, Ozturk *et al.* 2024, Li *et al.* 2024, Pourmohammadi *et al.* 2025).

Seepage-induced failures, including base heave and piping, are critical concerns in the stability of deep excavations, especially in sandy soils. These failures occur when upward seepage forces eliminate effective stress at the base, causing structural instability and posing safety hazards (Terzaghi 1925). Marsland (1953) used physical modeling to distinguish between base heave and piping by examining the effects of relative density and stress distribution. He found that piping typically begins at the wall tip in dense sands, while base heave occurs in loose sands when the pore pressure equals the vertical stress beneath the excavation.

In Terzaghi's classical formulation of base heave, the failure mechanism is idealized as a rectangular block of soil located approximately at a distance of D/2 behind a retaining structure embedded to a depth D, with the failure mass extending vertically by a height of D (Terzaghi 1925, Terzaghi and Peck 1968). This simplified representation, derived from two-dimensional model tests conducted in homogeneous, cohesionless soils, has been widely adopted in geotechnical engineering practice for evaluating basal stability conditions. The stress equilibrium within the potential failure zone is governed by Eq. (1).

$$h\gamma_w + D\gamma_w = (\Delta h_{av} + h + D)\gamma_w \tag{1}$$

where h denotes the height of the water column above the excavation base, γ_w is the unit weight of water, D is the embedment depth of the wall below the excavation level, and γ_{sat} represents the saturated unit weight of the soil. This relation equates the total vertical stress on the soil block with the upward water pressure acting at its base. Substituting $\gamma_{sat}=\gamma'+\gamma_w$ where γ' is the effective unit weight of the soil, yields the simplified form

$$D\gamma' = \Delta h_{av}\gamma_w \tag{2}$$

From this, the critical hydraulic gradient i_{cr} can be derived as

$$i_{cr} = \gamma'/\gamma_w = \Delta h_{av}/D \tag{3}$$

The initiation of base heave in cohesionless soils is primarily governed by the balance between upward-directed seepage forces and the submerged unit weight of the soil. This phenomenon is typically assessed using the critical hydraulic gradient, which marks the threshold at which seepage forces exceed the soil's submerged weight and initiate instability. When the average hydraulic gradient

*Corresponding author, Ph.D.
E-mail: subasi@tau.edu.tr

ISSN: 2005-307X (Print), 2092-6219 (Online)

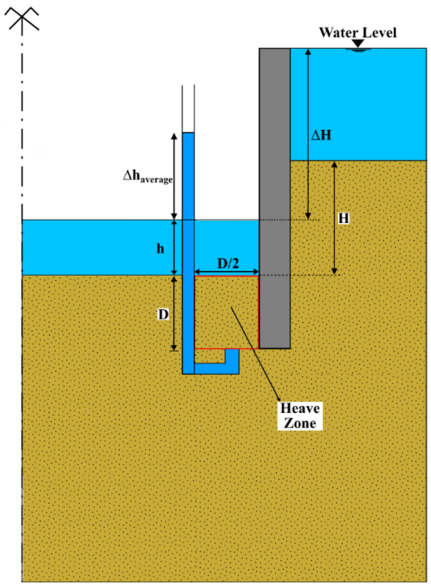

Fig. 1 Two dimensional Terzaghi seepage failure by heave (Terzaghi and Peck 1968)

measured in the field ($i_{av}=\Delta h_{av}/D$) surpasses the critical value ($i_{cr}=\gamma'/\gamma_w$), the effective stress at the excavation base may reduce to zero or become negative. Such conditions make the soil highly susceptible to uplift, deformation, and potentially piping failure. In highly permeable sandy soils, rapid buildup of pore water pressure under confined flow can trigger instability. Terzaghi's seepage failure model (Fig. 1) shows that heave occurs when upward seepage forces exceed the soil's submerged weight (Terzaghi and Peck 1968).

In conventional engineering practice, safety against base heave is evaluated by comparing the average hydraulic gradient acting within the heave zone to the soil's critical hydraulic gradient. If $i_{cr}>i_{av}$, the soil mass is deemed stable, as the submerged weight is sufficient to resist upward seepage. This criterion remains a fundamental component of preliminary stability checks in excavation design. However, real-world conditions often diverge significantly from the assumptions made in theoretical models. Variability in soil properties, anisotropic permeability, partial saturation, and non-uniform excavation geometries can all affect the pore pressure distribution in ways that classical approaches do not account for. As such, stability computations based solely on these simplified models may underestimate failure potential. A safety factor is introduced to address these uncertainties and is defined as $FS= i_{cr}/i_{av}$. A safety factor below an acceptable threshold suggests that remedial measures are necessary. One widely adopted strategy is to increase the embedment depth D of the retaining wall below the excavation base. A deeper embedment enhances both the resisting weight of the soil and the seepage path length, thereby improving overall stability. The optimal embedment depth depends on several factors, including excavation geometry, total head difference across the base, subsoil stratification, and boundary conditions of the surrounding groundwater system. Accurate determination of i_{av} requires a reliable estimate of the hydraulic head difference Δh_{av} at the base of the potential failure zone. This in turn requires the pore water pressure distribution within the soil mass. Accurate determination of i_{av} requires a reliable estimate of the hydraulic head difference Δh_{av} at the base of the potential failure zone. This in turn requires the pore water pressure distribution within the soil mass.

Classical studies made fundamental contributions to the understanding of seepage-induced instability through simplified analytical and physical models. As geotechnical engineering practice and computational capabilities advanced, these foundational approaches were refined and extended through numerical methods capable of capturing complex soil–water interactions with greater precision. Since the early 2000s, developments in coupled hydro-mechanical modeling and experimental validation have enabled researchers to analyze intricate boundary conditions and soil behaviors, including anisotropy, stratification, and partial saturation, with improved accuracy beyond the scope of classical theories. Building upon this progress, subsequent research has focused on overcoming the limitations of traditional approaches in representing realistic field conditions, particularly under three-dimensional seepage flow. For instance, Benmebarek *et al*. (2005) used FLAC-2D to simulate piping and base heave in sandy soils within a cofferdam and identified critical hydraulic gradients, underscoring the importance of accurate seepage modeling in design. Similarly, Koltuk *et al.* (2016) examined the sensitivity of the safety evaluation method in DIN EN 1997-1 to the definition of limit states. They proposed the hydraulic gradient as a more reliable design parameter and demonstrated that applying two-dimensional assumptions to three-dimensional geometries can result in localized failure zones resembling quicksand conditions. In a follow-up study, Koltuk and Azzam (2019) introduced the quicksand condition as a reliable design criterion for eliminating ambiguity in defining 3D failure geometries. Koltuk *et al.* (2015) also performed three-dimensional steady-state groundwater flow simulations in sheeted excavation pits using ABAQUS, demonstrating that safety factors can be up to 56% higher than those obtained from conventional two-dimensional Terzaghi-based analyses, depending on the b/D ratio and pit geometry. They further compared the Baumgart–Davidenkoff and Terzaghi failure criteria, highlighted the role of anisotropic permeability and model dimensions, and confirmed similar trends in stratified soils. Tu *et al.* (2023) advanced the theoretical understanding of tunnel face stability by proposing a three-dimensional rotational failure mechanism for inclined layered soils based on limit analysis. Their results demonstrated that increasing the dip angle of the soil interface significantly reduces the critical support pressure and induces asymmetric collapse patterns at the tunnel face. This framework provides an important link between classical limit analysis and realistic geological conditions, offering valuable insights for stability assessment in inclined stratified ground. Tu *et al*. (2024) complemented analytical research by integrating three-dimensional Discrete Element Method (DEM) simulations with large-scale physical model tests to investigate tunnel face stability

in sand–gravel inclined strata. Their findings revealed that the critical support pressure decreases as the inclination angle of the soil interface increases, and that DEM simulations closely reproduce the observed failure mechanisms from laboratory tests. This integrated experimental–numerical approach enhances predictive accuracy for tunnel face behavior in anisotropic granular media and provides valuable guidance for design and construction in inclined ground conditions.

The role of cohesion in seepage-induced failure has also been an important focus of recent investigations. Wudtke and Witt (2009) explored the effect of cohesion, revealing that even slight increases in cohesive strength raise the hydraulic gradient required for soil failure. They also found that failure is heavily influenced by the stress state, stratification, and saturation level. These findings underscore the need for cohesion-sensitive models in evaluating hydraulic heave. Furthermore, Zhou *et al*. (2021) proposed a new analytical formula for the critical hydraulic gradient of cohesive soils, incorporating shear strength effects. Their study demonstrated that soil thickness, failure radius, and shear strength significantly influence the critical gradient, with their formula aligning well with experimental data and achieving a maximum error of just 16%. Recent laboratory investigations by Di *et al.* (2024) demonstrated that seepage flow significantly alters the effective stress distribution at the tunnel face under saturated conditions. Their results showed that decreasing the water pressure ratio enlarges the collapse zone above the face, confirming the key role of pore pressure in face instability. These findings provide experimental evidence for refining stability criteria in submarine shield tunneling.

Accurate prediction of seepage behavior is dependent on reliable estimation of hydraulic parameters such as permeability. Farkas *et al.* (2019) addressed this issue by combining laboratory-scale physical models with numerical FEFLOW simulations to determine the permeability of medium-grained sands under different flow conditions. Their validated models showed strong agreement with experimental data, proving the feasibility of using calibrated simulations for real-world permeability estimation and seepage analysis. These findings contribute to improving the accuracy of seepage predictions in various geotechnical applications. Kaveh and Seddighian (2021) developed a hybrid method combining the Finite Element Method with five meta-heuristic algorithms to manage the complexities of seepage and seismic effects on slope stability. Their framework successfully identified critical failure surfaces and enhanced the reliability of safety factor estimations in multi-variable scenarios. This approach represents a robust tool for advanced geotechnical design. Additionally, Bensmaine *et al*. (2022) performed axisymmetric FLAC simulations to analyze seepage failures in cylindrical cofferdams. Their study identified various failure modes, including boiling, heaving, liquefaction, and passive pressure reduction, which are influenced by factors such as hydraulic head ratio, friction angle, dilatancy, and wall-soil interface properties. The findings confirm the significance of realistic geometries and material parameters in failure mechanisms, supporting the integration of advanced numerical methods in practical design. Nhu *et al*. (2024) carried out steady-state seepage simulations in earth dams founded on foliated rock using three-dimensional PLAXIS 3D LE software. They defined anisotropic permeability as a function of foliation dip and subdivided the dam axis into five flow zones for detailed analysis. Their results show that anticline zones convey more than twice the seepage rates of syncline areas, and that finger drains, while effective at channeling flow both longitudinally and vertically, are prone to blockage when compared against field piezometric measurements.

Seepage induced failure mechanisms in granular soils have also been a subject of significant investigation. Wang *et al.* (2022) studied seepage failure in sandy gravels and fine-grained sands, identifying four distinct phases in the failure process. They found a linear relationship between hydraulic gradient and seepage velocity during the early phases, which later becomes nonlinear as inertial forces dominate. This study challenges the applicability of Darcy's law in granular soils and clarifies the mechanisms behind seepage failure, offering new insights into the behavior of granular soils under seepage conditions. The stability of braced excavations in soft clays has been another area of focus in recent studies. Abdi and Ou (2023) employed three-dimensional finite element analysis with the strength reduction method to investigate failure mechanisms in braced excavations. Their model successfully validated wall displacements with observed field data from the Nicoll Highway collapse. The study revealed that excavation failure began from the yielding of the strut-waler connection, which was consistent with field observations. This approach demonstrates the applicability of the proposed finite element model for evaluating the stability of braced excavations in soft clays, further enhancing the accuracy of geotechnical design.

Taken together, these studies illustrate how the field has progressed from simplified analytical approaches to sophisticated, model-validated simulations that couple seepage mechanics with realistic soil behavior in both cohesionless and cohesive ground conditions. However, two-dimensional or purely cohesionless frameworks cannot fully capture the complex three-dimensional seepage fields encountered in real excavation projects. As a result, the failure surfaces and critical hydraulic gradients predicted by 2D analyses often deviate from observed field behavior, underscoring the need for advanced 3D finite-element modeling to reliably capture the hydro-mechanical interactions governing excavation stability under seepage. Despite these advances, existing analyses still lack a consistent understanding of how slight cohesive strength affects seepage-induced failure mechanisms in sandy ground under realistic three-dimensional excavation conditions.

A review of recent literature reveals that no comprehensive investigation into the effects of very low level cohesion on heave behavior within axisymmetric three-dimensional seepage analyses. Most existing studies have focused on two-dimensional conditions or on homogeneous, cohesionless sandy soils, with only a few addressing highly cohesive or stratified grounds. To fill this

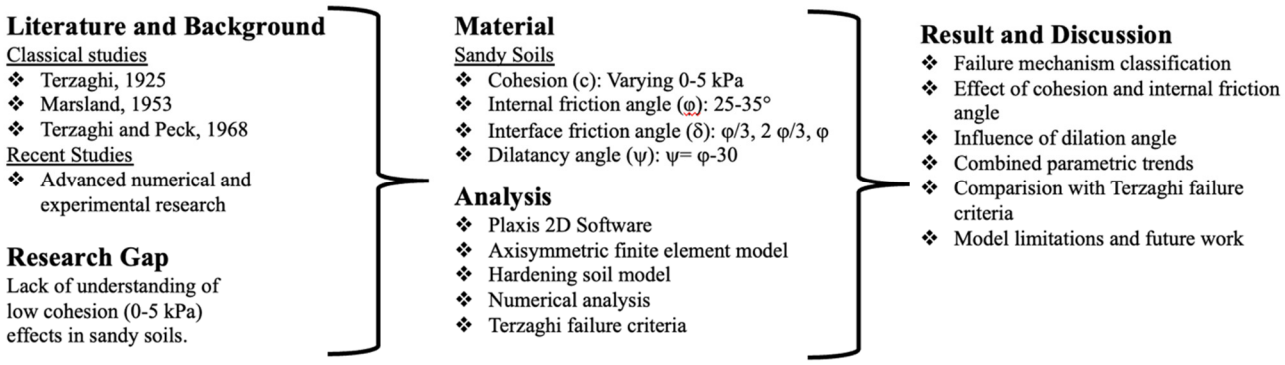

Fig. 2 The graphical abstract of this study

research gap, the present study performs the first systematic parametric investigation of cohesion values ranging from 0 to 5 kPa in an axisymmetric 3D geometry. By utilizing circular symmetry, the model reduces computational demands while enabling refined meshing and improved accuracy. This framework contributes to a more realistic understanding of seepage-induced heave and provides a basis for revising conventional stability assessment methods.

In practice, sandy soils that are nominally cohesionless may still develop measurable shear strength due to the presence of fine-grained particles such as silt or clay, which can enhance interparticle bonding. These fines-related mechanisms are often encountered in natural deposits and engineered backfills and may impart a small but significant degree of apparent cohesion, even under fully saturated conditions. Recognizing this, the present study considers a cohesion range of 0–5 kPa to realistically capture the stabilizing influence of such minor cohesive effects. This assumption enhances the geotechnical relevance of the findings.

The numerical simulations were conducted using a series of hydraulically coupled, axisymmetric finite-element analyses of circular sheeted excavation pits. The model configuration, material parameters, and boundary conditions are described as follows. Motivated by the recognized limitations of classical two-dimensional analytical solutions, the study proceeds with a series of hydraulically-mechanically coupled, axisymmetric finite-element analyses of circular sheeted excavation pits. The homogeneous sand layer is modeled with cohesion values from 0 to 5 kPa and internal friction angles between 25° and 35°, reflecting lightly cemented or fine-containing sandy soils. Interface friction between the retaining wall and surrounding soil is varied systematically (φ, $2\varphi/3$, $\varphi/3$), and—where $\varphi > 30°$—the dilation angle is computed as $\delta = \varphi - 30°$ and incorporated accordingly. The commonly adopted assumption of $\psi = \varphi - 30°$ for sands is grounded in both empirical and theoretical studies on stress-dilatancy behavior. This formulation reflects the typical dilative response observed in dense granular soils and has been applied in numerous finite element studies for modeling drained conditions (e.g., Bolton 1986, Schanz and Vermeer 1996). While simplified, this relationship offers a practical means of incorporating dilatancy effects in numerical simulations and aligns with observed trends in triaxial and plane strain tests. Numerical results are then compared with Terzaghi's classical theory to assess how slight cohesion alters both critical hydraulic conditions and failure-surface geometry, providing important insights into the stabilizing effect of minor cohesive strength under seepage-induced heave. The overall framework of the study, encompassing the literature background, material parameters, numerical modeling approach, and parametric evaluation, is schematically summarized in Fig. 2.

2. Finite element analysis

Finite element simulations in PLAXIS 2D Version 2024.2.0.1144 (2024) were used to model the failure mechanisms associated with base heave and piping induced by seepage. The numerical simulations account for the properties of a homogeneous sand layer, with varying dilation angle, cohesion and internal friction angles. Additionally, the interaction between the wall and soil is modeled with different friction values. Hardening soil model is adopted to better represent the non-linear behavior of the sand layer under the influence of seepage. The subsequent sections provide a detailed description of the numerical model, the hardening constitutive equations, and the various stages of the numerical analysis.

2.1 Numerical model

Hydro-mechanically coupled finite element analyses were carried out to evaluate the development of heave under seepage conditions in a circular excavation geometry. The numerical model prepared for this purpose is illustrated in Fig. 3. A simplified axisymmetric configuration was adopted to represent the three-dimensional site geometry (Fig. 3(a)). This approach was also employed to define the soil profile (Fig. 3(b)), accurately reflecting the geometry of the circular excavation. The model dimension were selected to minimize boundary effects during the analyses. To maintain hydrostatic balance, the upstream ground surface and the excavation base were assigned the same elevation. The embedment depth of the wall was defined as 4 meters.

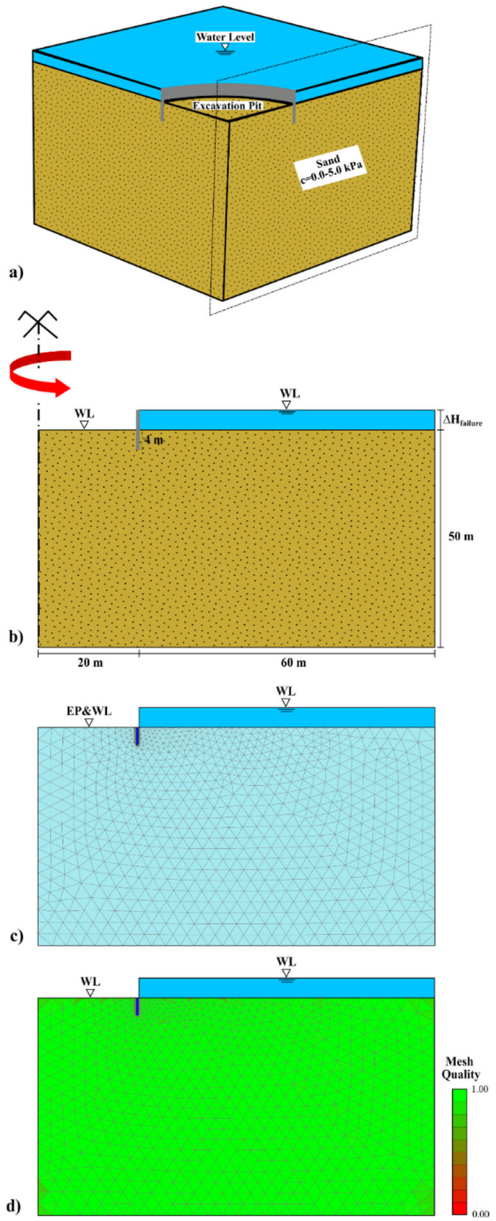

Fig. 3 Numerical analysis (a) 3D field conditions, (b) Axisymmetric soil profile, (c) Finite element model and (d) Mesh quality

The influence of mesh density on the numerical results was systematically evaluated as part of the modeling process. Mesh refinement up to and including the 'fine' density led to an increase in the computed $H_{Failure\text{-}FEM}$. However, further refinement to a 'very fine' mesh had a negligible impact on $H_{Failure\text{-}FEM}$ compared to the 'fine' mesh. The effect of mesh density on the failure mechanism shape was also found to be insignificant when at least a medium-density mesh was used. Based on these observations, a 'very fine' mesh consisting of 1506 triangular elements with 15 nodes per element, resulting in a total of 12330 nodes, as shown in Fig. 3(c), was adopted in all subsequent analyses to ensure accuracy and computational efficiency. The quality of the finite element mesh is presented in Fig. 3(d), where mesh quality ranges from 0 to 1.

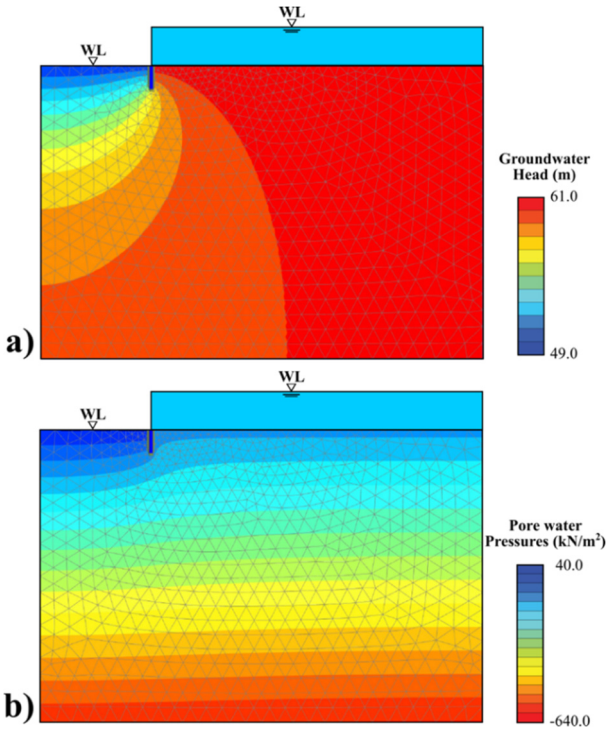

Fig. 4 Example of axisymmetric excavation pit in a homogeneous isotropic half-space for φ=30°, δ= 2φ/3, c= 3 kPa (a) Groundwater head and (b) Pore water pressure distribution

As shown, the mesh used in this study is of very high quality. This configuration provided a stable basis for evaluating seepage-induced deformations and failure mechanisms without introducing numerical artifacts. Accordingly, all parametric and comparative studies were conducted using this optimized mesh to ensure consistency and reliability across simulations.

In selecting the boundary conditions, the lateral boundaries were fixed in the horizontal direction, while the bottom boundary was fixed in both horizontal and vertical directions. The lateral and bottom boundaries of the model were assumed to be impermeable. The retaining wall was modeled as a rigid, impermeable plate with negligible thickness, fixed in place.

Fig. 4 illustrates the simulated potential drawdown and the corresponding pore-water pressure distribution for the axisymmetric excavation pit. The results clearly depict the reduction in hydraulic potential induced by the head difference across the retaining structure (Fig. 4(a)) and the associated redistribution of pore-water pressures within the soil mass (Fig. 4(b)). The numerical predictions exhibit close agreement with the expected hydro-mechanical response, indicating that the adopted modelling approach reliably captures both the seepage-induced potential field and the resulting pore-pressure regime.

2.2 Hardening constitutive equations

In the numerical analyses, the Hardening Soil (HS) model was adopted to simulate the elasto-plastic behavior of sandy soils, owing to its ability to capture stress-

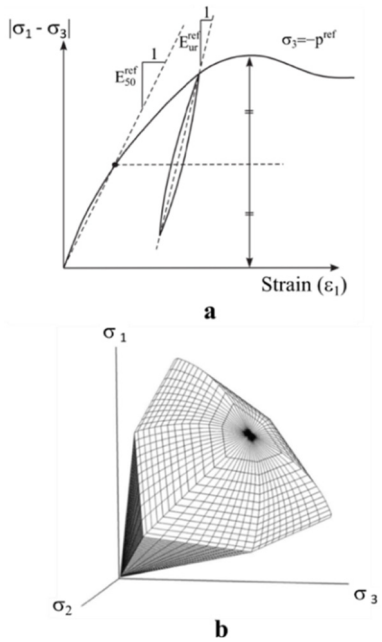

Fig. 5 Hardening soil model, (a) Definition of E_{50}^{ref} and E_{ur}^{ref},for drained triaxial test results (b) Representation of the total yield contour in principal stress space (Plaxis 2D Manuals 2025)

dependent stiffness and to distinguish between shear and volumetric hardening mechanisms. This advanced constitutive framework accounts for key soil behaviors such as consolidation, re-compression, and stiffness degradation with increasing stress, making it well suited for seepage conditions where loading and unloading occur simultaneously on opposite sides of an excavation. The model's capacity to differentiate stiffness responses during loading, unloading, and reloading ensures a more realistic representation of soil behavior under such complex hydraulic and mechanical conditions. (Song *et al.* 2024, Hu and Du 2025).

The Hardening Soil Model (HSM) defines the numerical limit state using key shear strength parameters such as the internal friction angle (φ), cohesion (c), and dilation angle (ψ) together with stiffness moduli that describe soil deformation behavior.

These stiffness parameters include the reference secant stiffness (E_{50}^{ref}), the unloading/reloading stiffness E_{ur}^{ref} and and the tangent stiffness obtained from oedometer loading E_{oed}^{ref} . While E_{50}^{ref} and E_{ur}^{ref} are typically derived from drained triaxial tests, E_{oed}^{ref} s obtained from oedometer tests, each referenced to a stress level of 100 kN/m². These parameters collectively enable a more realistic representation of soil behavior under complex loading conditions.

The stress-dependent behavior of the soil was represented using the Hardening Soil model, which incorporates both shear and volumetric hardening to simulate realistic stiffness degradation and plastic yielding under increasing load. As illustrated in Fig. 5, the Hardening Soil Model is conceptually represented through the definition of stiffness parameters from drained triaxial tests and the yield surface in principal stress space. These visualizations clarify the stress–strain behavior and plastic yielding characteristics adopted in the numerical analyses (Plaxis 2D Manuals 2025).

In this study, the dilation angle was set to zero, while the values of cohesion (c) and internal friction angle (φ) were adjusted according to the parametric study conducted. The parameters used in the analyses are given in Table 1.

Table 1 Hardening soil model parameters used in the numerical analyses

Parameter	Description	Unit	Method	Value/Definition
γ_{unsat}	Unsaturated unit weight	kN/m³	Assumed / Literature	18
γ_{sat}	Saturated unit weight	kN/m³	Assumed / Literature	20
c	Cohesion	kPa	Investigated in this study	0–5 kPa
φ	Internal friction angle	[°]	Investigated in this study	25°–35°
δ	Interface friction between wall and surrounding soil	[–]	Investigated in this study	φ/3, 2 φ/3, φ
ψ	Dilatancy angle	[°]	Investigated in this study	ψ= φ–30
E_{50}^{ref}	Reference secant stiffness (50% peak deviatoric stress)	kN/m²	Assumed / Literature	30000
E_{oed}^{ref}	Reference tangent stiffness from oedometer test	kN/m²	$E_{oed}^{ref}=E_{50}^{ref}$	30000
E_{ur}^{ref}	Unloading/reloading stiffness	kN/m²	$E_{ur}^{ref}=3xE_{50}^{ref}$	90000
m	Power for stress-level dependency of stiffness	[–]	Default	0.5
υ_{ur}	Poisson's ratio for unloading-reloading	[–]	Default	0.2
p^{ref}	Reference stress for stiffnesses	kN/m²	Default	100
K_0^{nc}	K_0 value for normal consolidation	[–]	$K_0^{nc}=1-\sin\varphi$	Depends on φ
R_f	Failure ratio q_f / q_a	[–]	Default	0.9
$\sigma_{tension}$	Tensile strength	kN/m²	Default	0

2.3 Parametric framework

Axisymmetric finite element analyses were conducted to assess the hydraulic stability of circular excavations. The model's geometric characteristics and Hardening Soil parameters are detailed in previous sections. Parametric analyses were performed to evaluate the effects of soil cohesion, internal friction angle, and interface friction, which are crucial for the stability of circular sheeted excavation pits under seepage conditions.

To assess the effect of minor cohesive strength on seepage-induced instability, the cohesion of the sand layer was varied from 0.0 to 5.0 kPa, with 0.5 kPa included to better represent effect of low cohesion level. This allowed a detailed evaluation of the transition between non-cohesive and weakly cohesive behavior. The internal friction angle was varied from 25° to 35° in 2.5° intervals, reflecting typical values for natural sands. For angles exceeding 30°, the dilation angle was calculated based on φ and incorporated as φ-30 in the analyses. The interface friction between the excavation structure and surrounding soil was modeled using three ratios of φ: φ, 2φ/3, and φ/3, to account for construction-related variations. This parametric framework enabled a robust evaluation of the influence of shear strength parameters and wall-soil interaction on the hydraulic stability of circular excavations under upward seepage conditions.

2.4 Numerical analysis stages

The numerical analysis, developed within a hydraulically–mechanically coupled finite element framework, was performed in two sequential stages to simulate the seepage-induced instability process in a controlled manner. In the first stage (K0 analysis), initial stress conditions were modeled with water levels placed at the top of the wall. In the second stage, the downstream water level was kept constant, while the upstream water level was gradually raised by 0.01 m. This process was continued until the model reached the ultimate (limit) state, indicating the onset of seepage-induced failure.

3. Result and discussion

This section first presents the three distinct failure patterns identified in our coupled hydro mechanical analyses: rectangular collapse zones, broader triangular bands extending toward the soil surface and surface localized failures and explains how each arises from variations in shear strength parameters. A total of 147 numerical simulations were conducted considering different combinations of input parameters.

The hydraulic potential differences obtained from numerical analyses without considering dilatancy are presented in Table 2. The corresponding results for cases where dilatancy occurs, that is, for internal friction angles exceeding 30°, are provided in Table 3. To assess the validity of the numerical model employed in this study, results obtained for cohesionless conditions (c = 0 kPa) were compared with previously published and verified numerical findings. Specifically, the critical hydraulic gradients and failure geometries produced under zero-cohesion conditions were found to be in close agreement with the finite element simulations reported by Koltuk *et al.* (2022) and the finite difference analysis by Benmarek *et al*. (2020). This consistency confirms that the modeling approach accurately captures the mechanisms of seepage-induced instability in sandy soils.

Building on this validation, the model was subsequently extended to explore the influence of low apparent cohesion (<5 kPa), a parameter range that has received limited attention in the literature. While no direct experimental data exist for this cohesion range, the validation under c = 0 kPa conditions offers a reliable basis to interpret the extended simulations. This approach enables a systematic investigation of how minor cohesive strength alters failure patterns and critical hydraulic conditions under seepage loading. The results demonstrate that small increases in cohesion enhance the resistance of sandy soils and lead to systematic shifts in failure geometry and in the critical hydraulic gradient. Subsequent analysis isolates the effect of internal friction angle on stability and examines interface friction under different parameter combinations. A detailed evaluation of dilation angle effects highlights its role in triggering and developing base heave. These insights are then integrated to identify the combined trends that control pit stability under seepage loading. The section closes with a critical review of model assumptions and recommendations for future work on non-circular geometries, stratified soil profiles and analyses calibrated against field data. Overall, the findings show that even modest increases in cohesion can significantly raise the threshold for seepage induced failure and underscore the need to revisit traditional cohesionless design.

Table 2 Hydraulic potential differences obtained from parametric seepage analyses under varying parameters

c	φ=25.00°			φ=27.50°			φ=30.00°			φ=32.50°			φ=35.00°		
(kPa)	δ=φ/3	δ=2φ/3	δ=φ	δ=φ/3	δ=2φ/3	δ=φ	δ=φ/3	δ=2φ/3	δ=φ	δ=φ/3	δ=2φ/3	δ=φ	δ=φ/3	δ=2φ/3	δ=φ
0.00	8.43	8.44	8.49	8.53	8.55	8.56	8.55	8.60	8.63	8.64	8.67	8.71	8.67	8.72	8.76
0.50	8.77	8.78	8.89	8.84	8.87	8.98	8.87	8.92	9.04	8.90	8.94	9.08	8.98	8.99	9.13
1.00	9.07	9.17	9.33	9.09	9.21	9.44	9.16	9.28	9.53	9.17	9.32	9.59	9.23	9.36	9.63
2.00	9.70	9.93	10.00	9.77	10.02	10.22	9.83	10.08	10.33	9.91	10.11	10.39	9.94	10.21	10.47
3.00	10.17	10.56	10.65	10.27	10.66	10.70	10.34	10.72	10.86	10.36	10.75	10.91	10.41	10.89	10.93
4.00	10.56	10.79	10.85	10.58	10.85	10.95	10.61	10.89	11.01	10.63	10.92	11.11	10.67	11.06	11.15
5.00	10.70	10.85	10.92	10.86	11.12	11.16	10.91	11.18	11.20	10.93	11.20	11.26	10.97	11.27	11.37

c: Cohesion (kPa), φ: Internal friction angle (°), δ: Interface friction between wall and surrounding soil

Table 3 Effect of dilatancy angle on critical hydraulic potential differences under varying parameters

c (kPa)	ψ=2.50°			ψ=5.00°		
	δ=φ/3	δ=2φ/3	δ=φ	δ=φ/3	δ=2φ/3	δ=φ
0.00	8.66	8.70	8.80	8.75	8.78	8.98
0.50	8.94	8.97	9.15	9.00	9.05	9.34
1.00	9.20	9.37	9.65	9.30	9.40	9.71
2.00	9.93	10.48	10.51	9.99	10.29	10.62
3.00	10.38	10.95	11.02	10.50	11.02	11.14
4.00	10.69	11.13	11.17	10.78	11.12	11.23
5.00	10.99	11.32	11.37	11.01	11.30	11.42

c: cohesion (kPa), φ: Internal friction angle (°), δ: Interface friction between wall and surrounding soil, ψ: Dilatancy angle (°)

3.1 Failure mechanism classification

In field practice, once impermeable diaphragm walls are in place, only the groundwater within the excavation pit is discharged, preserving the external groundwater level and creating a suitable dry working environment. However, this process generates a hydraulic head difference that drives seepage flow from the upstream side into the pit. As seepage advances, pore water pressure at the excavation base increases, leading to a reduction in effective stress. Under these conditions, mechanisms such as heave, piping and internal erosion may develop, potentially undermining the overall stability of the pit.

Fig. 6 illustrates three distinct failure patterns revealed by the numerical analyses. Similar failure modes have also been observed in previous studies by Wudtke and Witt (2006) and Koltuk *et al*. (2022). In addition to the overall failure geometries, the corresponding distributions of plastic points are also presented in the figure.

These results indicate three characteristic patterns of plastic point concentration, each associated with a specific failure mechanism, providing deeper insight into the progression and extent of instability zones within the soil mass.

According to Fig. 6, the first pattern features a narrow, rectangular-shaped collapse zone. The second appears as a wider, triangular-shaped band extending toward the soil surface. The third is limited to the surface and its immediate vicinity. These patterns emerged under different combinations of φ and δ, with cohesion acting as the key controlling parameter. As cohesion increased, a clear progression from the rectangular collapse toward failure localized at the surface was observed.

3.2 Effect of cohesion and internal friction angle

A comprehensive series of parametric analyses was conducted to examine the influence of soil cohesion and internal friction angle on seepage-induced failure mechanisms. The internal friction angle (φ) was varied between 25° and 35°, while the wall–soil interface friction

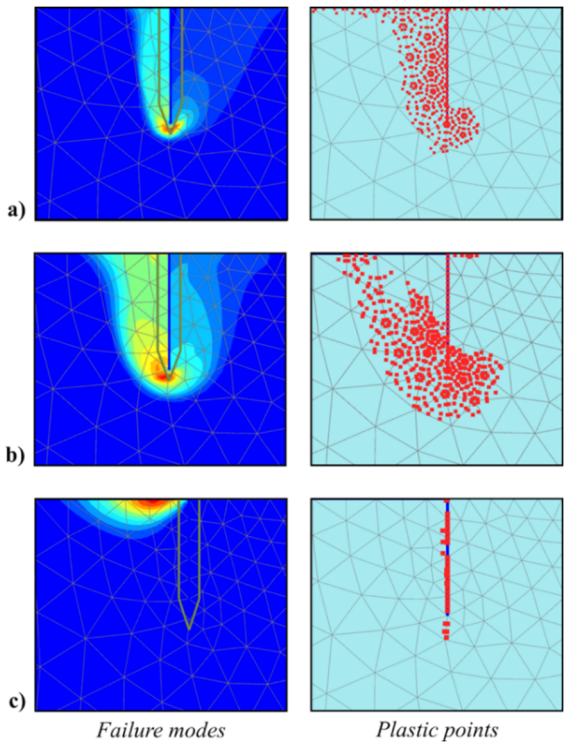

Fig. 6 Failure zones obtained from the numerical analyses (a) Rectangular shaped, (b) Triangular shaped and (c) Surface failure

(δ) was analyzed in three configurations: φ⁄3, 2φ⁄3, and φ. Although simulations were performed for the full range of φ values, the failure mechanisms corresponding to the two limiting cases (φ = 25° and φ = 35°) are presented in Figs. 7-12 to clearly illustrate the representative trends. These results reveal how variations in φ and δ jointly influence the geometry and extent of the failure zones, and how increasing cohesion alters the hydraulic potential distribution and enhances overall stability against seepage-induced heave.

In Figs. 7-9, the influence of cohesion on the failure mechanism is evaluated alongside the governing shear strength parameters φ and δ. Cohesion acts as a decisive parameter that determines whether the collapse develops as a rectangular band, a triangular wedge, or a surface-localized failure. Under low internal friction (φ = 25°) and

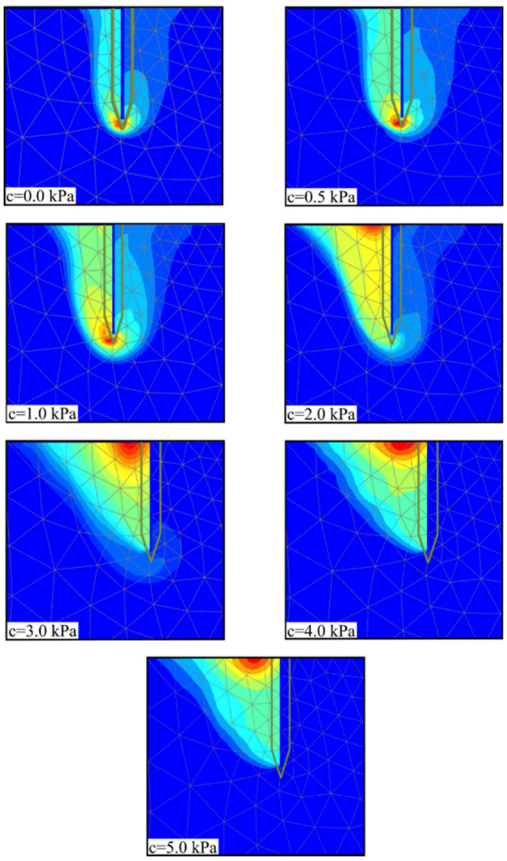

Fig. 7 Variation in failure mechanism with increasing soil cohesion for φ = 25° and δ = φ/3

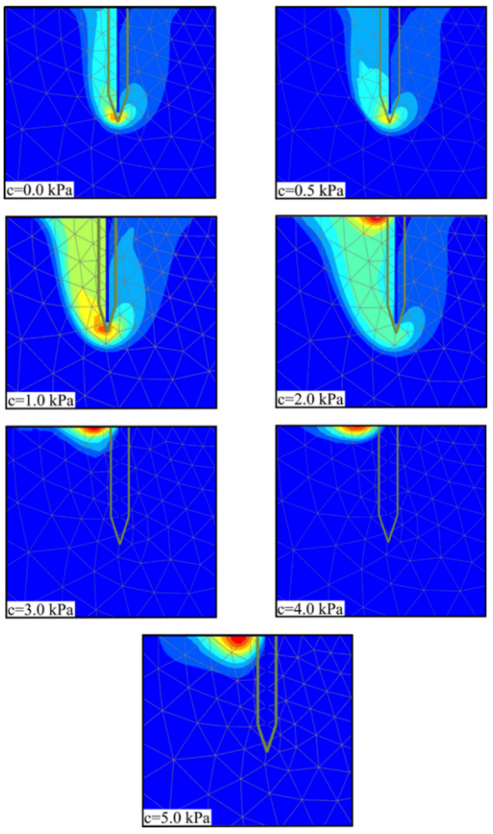

Fig. 8 Variation in failure mechanism with increasing soil cohesion for φ = 25° and δ = 2φ/3

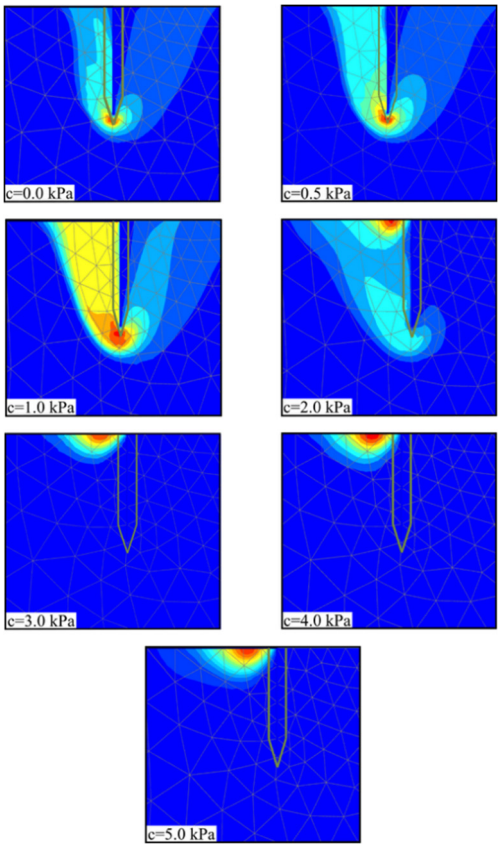

Fig. 9 Variation in failure mechanism with increasing soil cohesion for φ = 25° and δ = φ

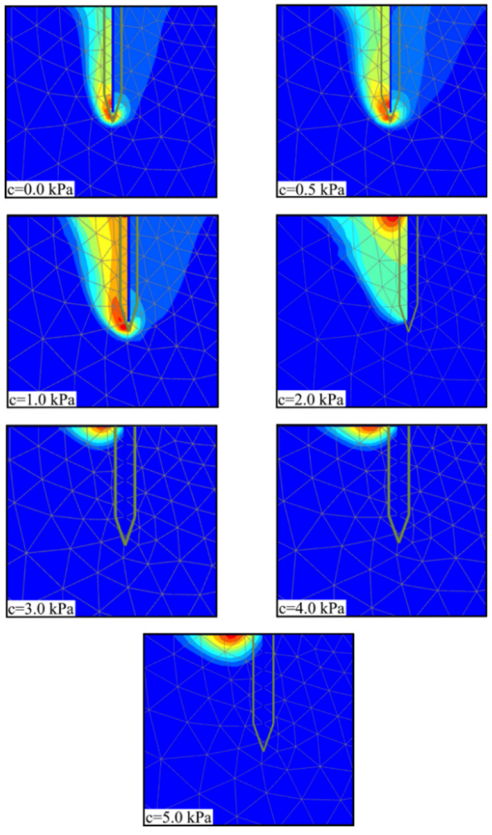

Fig. 10 Variation in failure mechanism with increasing soil cohesion for φ = 35° and δ = φ/3

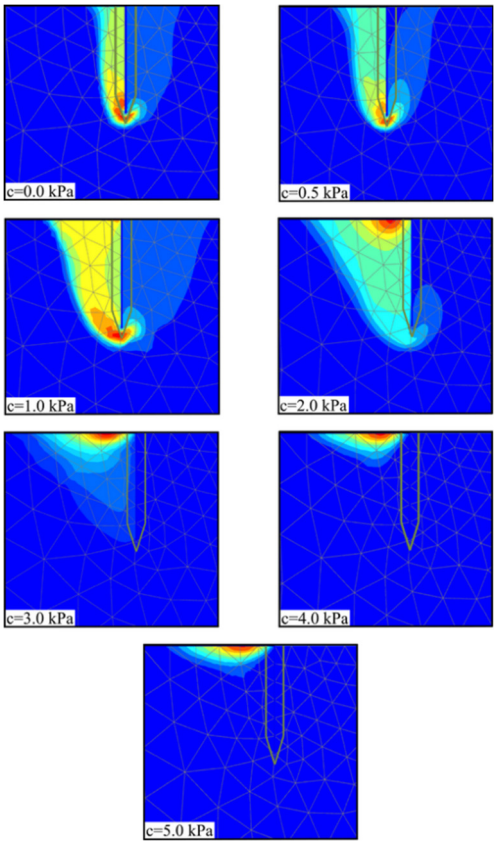

Fig. 11 Variation in failure mechanism with increasing soil cohesion for φ = 35° and δ = 2φ/3

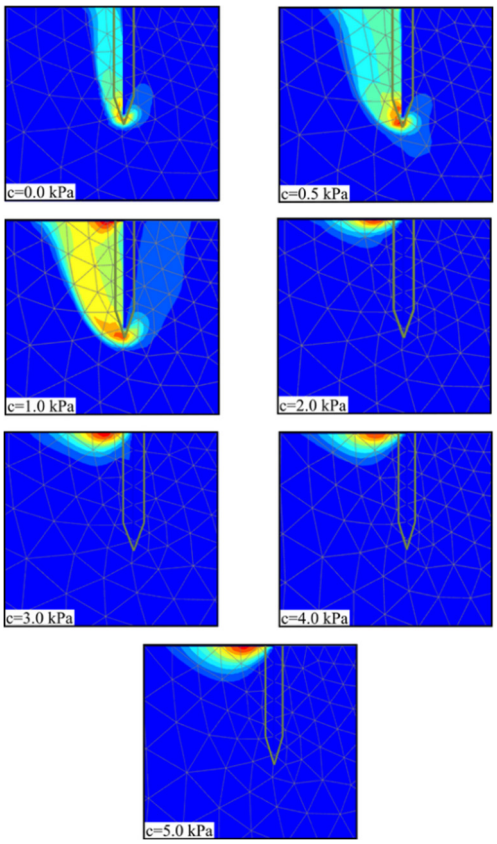

Fig. 12 Variation in failure mechanism with increasing soil cohesion for φ = 35° and δ = φ

weak interface shear (δ = φ⁄3), zero cohesion results in a narrow, sub-base rectangular collapse zone. As cohesion exceeds approximately 2 kPa, the triangular failure mode becomes dominant, and surface-localized failure emerges when cohesion reaches about 4 to 5 kPa. Increasing δ to 2φ⁄3 at the same φ markedly reduces these thresholds—the triangular pattern forms at around 1 kPa, and surface failure begins near 3 kPa. When the wall–soil interface is fully mobilized (δ = φ), even 0.5 kPa of cohesion eliminates the rectangular mode in favor of a triangular wedge, while cohesion above 2 kPa produces immediate surface collapse. These results demonstrate that in coupled hydro-mechanical systems, small increases in cohesion can fundamentally alter both the mechanism and geometry of failure.

When φ increases to 35°, the transition between failure modes occurs at substantially lower cohesion levels, as illustrated in Figs. 10-12. For δ = φ/3 and δ = 2φ/3, the change from triangular to surface failure initiates near 2 kPa of cohesion, while for δ = φ, this occurs at approximately 1 kPa. Cohesion values exceeding 2 kPa lead to complete surface failure. These results confirm that cohesion enhances stability but also serves as the main parameter controlling failure geometry. Elevated internal and interface friction angles reduce the cohesion threshold required to shift from deep-seated to surface-type failure, highlighting the necessity of incorporating even low cohesion values in design assessments for sandy excavations.

In our numerical simulations cohesion proves to be the dominant factor in determining whether sandy soil layers will experience a rectangular, triangular or surface-localized failure when compared with changes in internal friction angle and wall–soil interface friction. As cohesion rises the failure pattern shifts first to a triangular form and then to surface failure. With low friction and weak interface interaction sandy layers typically collapse in a rectangular mode while high friction and strong wall–soil coupling cause even small cohesion increases to produce surface failures. Increasing the internal friction angle further reduces the cohesion level needed to trigger triangular or surface collapse. These findings reinforce the conclusion that the internal friction angle and interface friction between the soil and wall are critical parameters governing failure mechanisms in seepage-related stability problems. While cohesion is often considered negligible for sandy soils, the present study shows that even small cohesion values can significantly affect failure surface geometry. These results show that in practical design the influence of cohesion must be considered not only by its magnitude but together with soil friction properties and interface shear characteristics.

3.3 Influence of dilation angle

To examine the influence of dilation on failure mechanisms, failure surface shapes were analyzed at cohesion values of 0 and 5 kPa, with internal friction angle φ = 35°, interface friction angle δ = φ, and dilation angle (ψ) of 5°, as shown in Fig. 13. At c = 0 kPa (Fig. 13(a)), the failure zone evolves from a narrow rectangular shape to a broader surface-type failure with increasing dilation. At c = 5 kPa (Fig. 13(b)), the failure surface remains more

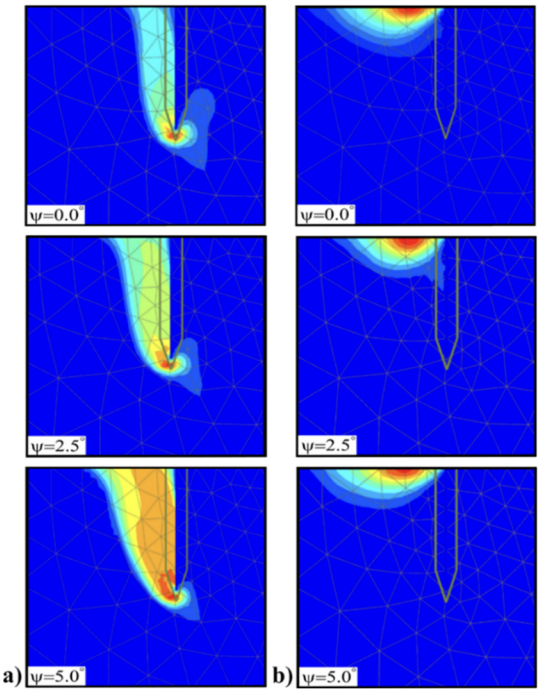

Fig. 13 Effect of soil cohesion change on the shape of the failure plane (φ=35° and δ=φ)

confined, yet dilation still promotes the transition toward surface-type failure. Increased cohesion clearly limits failure spread, enhancing overall stability.

As illustrated in Fig. 13, these results highlight the combined effect of cohesion and dilation on the evolution of failure surface geometry. The transition from a localized failure pattern to a more distributed surface-type mechanism becomes increasingly evident in soils with greater cohesion, emphasizing the significance of both parameters in capturing realistic failure behavior. Reliable modeling of this interaction necessitates advanced constitutive formulations capable of representing the coupled effects of shear strength, volumetric deformation, and interface behavior. Incorporating these aspects into numerical simulations enhances the accuracy of seepage-induced failure predictions in practical geotechnical engineering applications.

3.4 Combined parametric trends

Following 105 numerical simulations, the potential differences induced by the groundwater level drop between the excavation base and the surface (ΔH_{FEM}) were evaluated by direct comparison with the critical value predicted by Terzaghi's method. The critical potential difference according to Terzaghi's approach was calculated as $\Delta H_{Terzaghi}$ = 8.8 m using Eq. (3). To assess how the coupled hydro-mechanical model compares with classical theory, the hydraulic head differences obtained from the finite-element simulations (ΔH_{FEM}) were normalized by $\Delta H_{Terzaghi}$. This normalization enables us to assess how cohesion (c), internal friction angle (φ) and interface friction angle (δ) alter the critical groundwater head difference responsible for failure in sandy soils, extending beyond Terzaghi's rectangular failure zone assumption. The resulting ratios $\Delta H_{FEM}/\Delta H_{Terzaghi}$ are plotted in Fig. 14 as functions of c, φ and δ.

The analyses reveal that soil cohesion (c) has a pronounced impact on the normalized hydraulic head difference ($\Delta H_{FEM}/\Delta H_{Terzaghi}$). Even a marginal increase in cohesion from 0 to 0.5 kPa leads to a measurable improvement in the normalized ratio, underscoring the importance of accounting for minor cohesive effects in the assessment of sandy soils. As cohesion increases from 0 to 5 kPa, the normalized ratio exhibits a steady upward trend across all tested values of internal friction angle (φ) and interface friction angle (δ). For example, at φ = 30° and δ = 2φ/3, the ratio increases from 0.98 at c = 0 to 1.27 at c = 5 kPa, reflecting a 29% enhancement in hydraulic resistance. These results suggest that slightly cemented sands, silty sands, or sands exhibiting apparent cohesion due to capillarity may offer significantly greater resistance to upward seepage than predicted by classical analytical approaches

Although cohesion exerts the dominant influence, the internal friction angle (φ) also contributes positively to hydraulic stability. Across all levels of cohesion, an increase in φ from 25° to 35° results in moderate yet consistent gains in the normalized ratio. For example, at c = 2 kPa and δ=2φ/3, $\Delta H_{FEM}/\Delta H_{Terzaghi}$ increases from 1.13 to 1.16. This effect becomes more pronounced when accompanied by higher cohesion values, emphasizing the synergistic role of frictional and cohesive components in resisting failure mechanisms such as base heave and piping.

The influence of the soil–structure interface friction angle (δ) was also systematically investigated. For a given set of cohesion and friction angle values, increasing δ from φ/3 to φ resulted in measurable, though comparatively modest, improvements in hydraulic resistance. As an illustrative example, at φ = 30° and c = 3 kPa, the normalized ratio increased from 1.18 to 1.23 as δ varied from φ/3 to φ. While less influential than cohesion, this result nonetheless underscores the beneficial effect of enhanced soil–structure interaction and its contribution to the overall hydraulic stability of the excavation system.

As presented in Fig. 15, the influence of cohesion and dilation angle on hydraulic stability is depicted through two comparative scenarios: one with an internal friction angle of 32.5° and the other with 35.0°.

These visualizations illustrate how variations in both parameters affect failure surface development and the corresponding hydraulic response. The dilation angle in each case was set to 5°, while δ was assumed equal to φ. The figure highlights progressive changes in failure geometry and normalized hydraulic head difference with increasing shear strength and dilation. These results serve as a visual benchmark for evaluating the interplay between strength parameters and hydraulic uplift resistance in cohesionless to slightly cohesive soils.

The numerical findings, as illustrated in Fig. 15, reveal that incorporating a nonzero dilation angle produces a marked improvement in hydraulic resistance, especially when the internal friction angle exceeds 30°. For example, at φ = 35° and δ = φ, the introduction of a 5° dilation angle

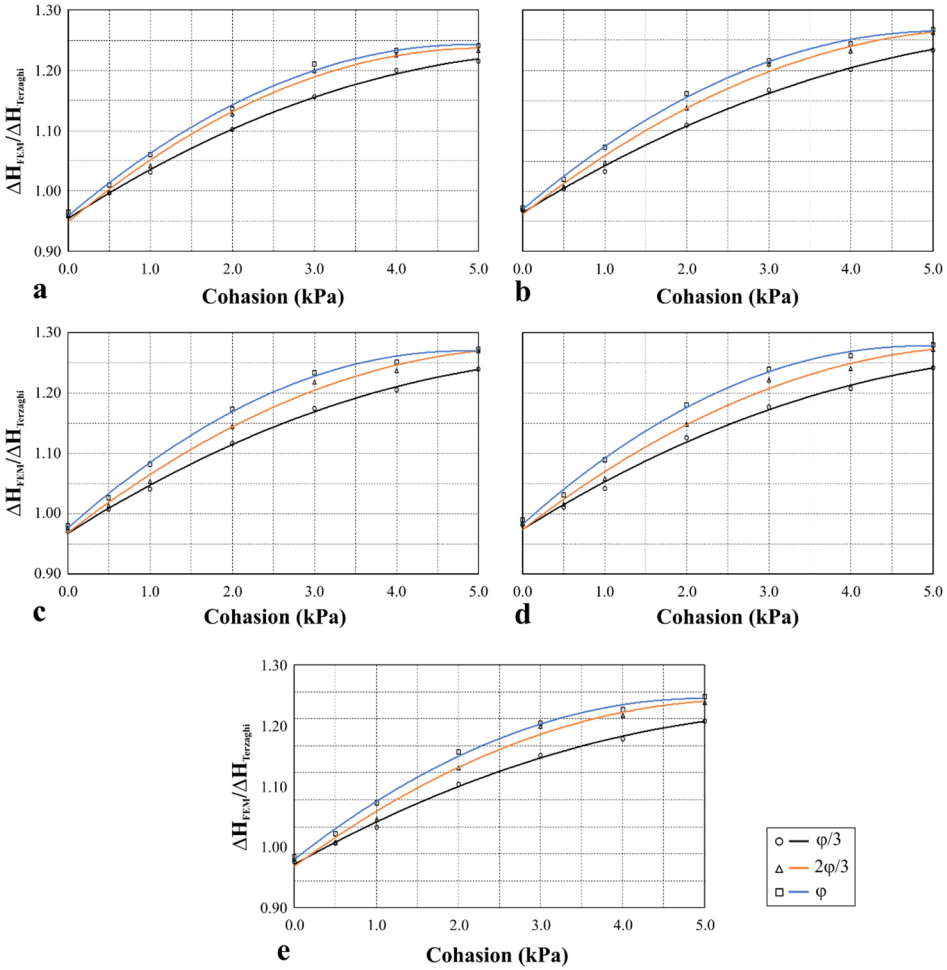

Fig. 14 Effect of cohesion depend on numerical analysis (a) 25.0°, (b) 27.5°, (c) 30.0°, (d) 32.5° and (e) 35.0°.

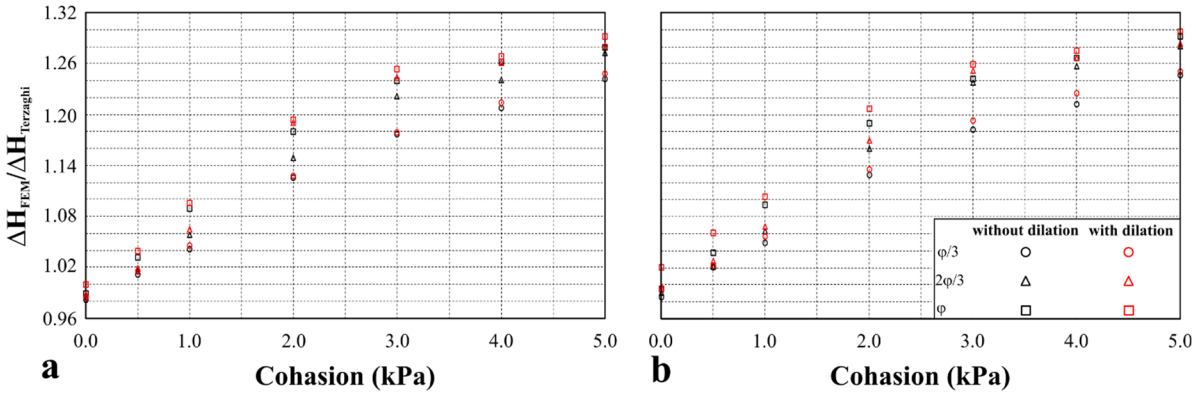

Fig. 15 Effect of cohesion and dilatation depend on numerical analysis (a) 32.5° and (b) 35.0°

leads to a higher normalized hydraulic head difference compared to the non-dilative case. This enhanced shear strength and resistance to seepage-induced failure underscores the importance of accounting for dilation in advanced geotechnical modeling. Moreover, these outcomes suggest that even small adjustments in cohesion, dilation, and interface friction can yield more accurate and less conservative design predictions for deep excavations and hydraulic loading conditions.

3.5 Model limitations and future work

This study employed three-dimensional coupled hydro-mechanical simulations, utilizing the axisymmetric simplification made possible by the circular geometry of sheeted excavation pits. The model incorporated anisotropic permeability conditions to reflect more realistic seepage behavior. A systematic parametric analysis demonstrated that even minor cohesive strength, often disregarded in conventional sandy soil design, can significantly improve

hydraulic stability. Incorporating directional permeability further enhanced the representativeness of the simulations with respect to field conditions.

Despite these strengths, the modeling framework is subject to certain limitations. The axisymmetric assumption is valid exclusively for perfectly circular geometries and may not adequately represent failure mechanisms in rectangular or irregular-shaped excavations. Additionally, the soil domain was modeled as a single, homogeneous sandy layer, whereas real geotechnical profiles frequently contain stratified layers, including impermeable or low-permeability clay lenses with varying degrees of cohesion. Such heterogeneity can significantly influence seepage pathways and alter the shape and location of failure surfaces. As a result, direct extrapolation of the findings to complex field conditions should be approached with caution.

To broaden the applicability and robustness of the results, future research should consider the following directions:

- Conduct fully three-dimensional simulations on non-circular geometries using plate-based or unstructured boundary modeling approaches to capture irregular excavation conditions more accurately.
- Incorporate stratified soil profiles with spatially variable permeability and cohesion to assess how geological layering influences seepage-driven heave and piping.
- Evaluate the impact of partially saturated conditions and transient flow to reflect more realistic groundwater behavior under variable hydraulic loading.
- Calibrate numerical predictions with experimental data, including field measurements and borehole tests, to validate the model's assumptions and strengthen its practical relevance.
- Investigate the interaction between structural elements and soil behavior under coupled seepage and mechanical loading to inform design standards for excavation support systems.

Pursuing these directions will help extend the insights gained from this study to a wider range of geotechnical scenarios and support the development of more robust design frameworks that account for the subtle yet stabilizing effects of low cohesion in sandy soils.

4. Conclusions

This study examines the significant influence of low soil cohesion on seepage-induced failure mechanisms in sandy soils, particularly base heave in excavation pits. Hydraulically-mechanically coupled, axisymmetric finite element analyses showed that even small cohesion values, ranging from 0 to 5 kPa, significantly affect the geometry of failure surfaces. Cohesion increased the critical hydraulic gradient for failure, improving stability and causing the failure surface to transition from rectangular to triangular, and eventually to surface-type. The inclusion of dilation angles, especially for internal friction angles over 30°, further enhanced this effect, demonstrating the critical role of dilation in failure patterns. These findings suggest that sands with minor cohesion, whether due to capillarity, fines content, or partial cementation, resist seepage-induced uplift more than classical models predict.

In sandy soils, the internal friction angle (φ) and the soil–structure interface friction angle (δ) are the primary factors governing stability under seepage conditions. However, the presence of even a small amount of cohesion also plays a significant role, particularly in influencing the geometry of failure surfaces and the critical hydraulic gradient. The addition of dilation effects strengthened these results, showing that even small variations in dilation, alongside cohesion and friction, significantly impact failure behavior. The findings of this study offer valuable guidance for practical geotechnical design. In sandy or silty sand deposits where minor apparent cohesion may develop due to the presence of fine particles or partial cementation, assuming a completely cohesionless condition may result in overly conservative designs. The numerical analyses demonstrate that even very small cohesion values, below 5 kPa, can significantly increase hydraulic stability against seepage-induced heave. For this reason, laboratory investigations that aim to determine the minor cohesive strength of such soils are recommended, as they can provide a more accurate basis for evaluating stability. Incorporating these measured values into design procedures, either by refining the factor of safety or by adjusting the critical hydraulic gradient, can enhance both reliability and cost efficiency. Overall, the study presents a preliminary framework for incorporating the effects of low-level cohesion into modern geotechnical design practice, contributing to safer and more realistic engineering solutions.

References

Abdi, A.S. and Ou, C.Y. (2023), "Failure investigation of braced excavation in soft clays: case study on the collapse of nicoll highway", *Proceedings of the 2nd International Symposium on Civil Engineering and Environmental Research,* Banjarmasin, Indonesia, October.

Benmebarek, N., Benmebarek, S. and Kastner, R. (2005), "Numerical studies of seepage failure of sand within a cofferdam", *Comput. Geotech.*, **32**(4), 264-273. https://doi.org/10.1016/j.compgeo.2005.03.001.

Bensmaine, A., Benmebarek, N. and Benmebarek, S. (2022), "Numerical analysis of seepage failure modes of sandy soils within a cylindrical cofferdam", *Civil Eng. J.*, **8**(7), 1388-1405. https://doi.org/10.28991/CEJ-2022-08-07-03.

Bentley Systems. (2024), PLAXIS 2D (Version 2024.2.0.1144) [Computer software]. Bentley Systems, Inc. https://www.bentley.com/plaxis.

Bolton, M.D. (1986), "The strength and dilatancy of sands", *Geotechnique*, **36**(1), 65-78. https://doi.org/10.1680/geot.1986.36.1.65.

Di, Q., Li, P., Zhang, M., Jia, Y., Li, S. and Cui, X. (2024), "Experimental study on the effect of seepage flow on the tunnel face stability in the saturated ground", *Ocean Eng.*, **299**, 117074. https://doi.org/10.1016/j.oceaneng.2024.117074.

Farkas, D., Hajnal, G. and Vasvári, V. (2019), "Validation of a physical and numerical model to solve problems of seepage flow", *Periodica Polytech. Civil Eng.*, **63**(2), 388-400.

https://doi.org/10.3311/PPci.12592.
Hu, J. and Du, Q. (2025), "Parameter study and engineering verification of the hardening soil model with small-strain stiffness for loess in the Xi'an area", *Appl. Sci.*, **15**(3), 1278. https://doi.org/10.3390/app15031278.
Kaveh, A. and Seddighian, M.R. (2021), "Optimization of slope critical surfaces considering seepage and seismic effects using finite element method and five meta-heuristic algorithms", *Periodica Polytech. Civil Eng.*, **65**(2), 425-436. https://doi.org/10.3311/PPci.17098.
Koltuk, S. and Azzam, R. (2019), "Use of quicksand condition to assess the base stabilities of sheeted excavation pits against seepage failure in cohesionless soils", *Arabian J. Sci Eng.*, **44**(10), 8515-8526. https://doi.org/10.1007/s13369-019-03890-y.
Koltuk, S. and Fernandez-Steeger, T. (2022), "Evaluation of seepage failure by heave in homogeneous cohesionless soils using finite element method", *Int. J. Geotech. Eng.*, **16**(10), 1201-1210. https://doi.org/10.1080/19386362.2022.2042965.
Koltuk, S., Fernandez-Steeger, T.M. and Azzam, R. (2015), "A numerical study on the seepage failure by heave in sheeted excavation pits", *Geomech. Eng.*, **9**(4), 513-530. https://doi.org/10.12989/gae.2015.9.4.513.
Koltuk, S., Fernandez-Steeger, T.M. and Azzam, R. (2016), "Investigations on hydraulic heave in foundation pits excavated in homogeneous soils", *Grundwasser*, **21**(3), 203-215. https://doi.org/10.1007/s00767-015-0309-5
Li, K., Chen, S., Zhao, P. and Pei, R. (2024), "Theoretical and numerical simulation analysis of the control effect of isolation piles on surface settlement induced by foundation pit excavation", *Geomech. Eng.*, **39**(3), 227-240. https://doi.org/10.12989/gae.2024.39.3.227.
Marsland, A. (1953), "Model experiments to study the influence of seepage on the stability of a sheeted excavation in sand", *Géotechnique*, **3**(6), 223-241. https://doi.org/10.1680/geot.1953.3.6.223.
Nhu, T.Q., Kunsuwan, N., Mairaing, W., Kunsuwan, B. and Chalermpornchai, T. (2024), "Behavior of seepage in earth dams through complex foundations using three-dimensional finite element method", *Geomech. Eng.*, **39**(3), 273-282. https://doi.org/10.12989/gae.2024.39.3.273.
Ozturk, B., Hussein, A.F., El Naggar, M.H. and Chen, H. (2024), "Seismic response of a model soil-pile-bridge system in cohesive soil", *Soil Dyn. Earthq. Eng.*, **187**, 109013. https://doi.org/10.1016/j.soildyn.2024.109013.
Plaxis 2D Manual (2025), Plaxis 2D Material Models Manual, Bentley System, Pennsylvania, USA.
Pourmohammadi, K., Khalkhali, A.B., Dabiri, R. and Adeli, M.M. (2025), "Experimental and numerical study of weak soil layer effects on ultimate bearing capacity of strip foundations resting on inclined layered soil masses", *Geomech. Eng.*, **41**(5), 481-491. https://doi.org/10.12989/gae.2025.41.5.481.
Sarvesha, R., Srinivasan, V. and Patelb, A. (2023), "Elastic settlements of identical angular footings in close proximity", *Geomech. Eng.*, **32**(2), 193-207. https://doi.org/10.12989/gae.2023.32.2.193.
Schanz, T. and Vermeer, P.A. (1996), "Angles of friction and dilatancy of sand", *Géotechnique*, **46**(1), 145-151. https://doi.org/10.1680/geot.1996.46.1.145.
Song, B., Liu, J. Y., Liu, Y. and Hu, P. (2024), "Generalization and implementation of hardening soil constitutive model in ABAQUS code", *Geomech. Eng.*, **36**(4), 355-366. https://doi.org/10.12989/gae.2024.36.4.355.
Terzaghi, K. (1925), "Erdbaumechanik Auf Bodenphysikalischer Grundlage", Franz Deuticke-Verlag, Leipzig and Wien, Germany/Austria.
Terzaghi, K. and Peck, R.B. (1968), Soil Mechanics in Engineering Practice, John Wiley & Sons, New York, NY, USA.
Tu, S., Li, W., Zhang, C. and Chen, W. (2023). "Effect of inclined layered soils on face stability in shield tunneling based on limit analysis", *Tunn. Undergr. Sp. Tech.*, **131**, 104773. https://doi.org/10.1016/j.tust.2022.104773.
Tu, S., Li, W., Zhang, C., Liu, T., Wang, L. and Jin, Z. (2024), "Model test and discrete element method simulation of tunnel face stability in sand-gravel inclined layered stratum", *Comput. Geotech.*, **172**, 106456. https://doi.org/10.1016/j.compgeo.2024.106456.
Wang, Y., Duan, X., Gu, Y. and Wang, S. (2022), "Experimental investigation of the seepage-induced failure process in granular soils", *Geofluids*, **2022**(1), 5703151. https://doi.org/10.1155/2022/5703151.
Wudtke, R.B. and Witt, K.J. (2006), "A static analysis of hydraulic heave in cohesive soil", *Proceedings of the 3rd International Conference on Scour and Erosion*, Amsterdam, Netherlands November.
Wudtke, R.B. and Witt, K.J. (2009), "Cohesive soil resistance and hydraulic heave at excavations", *Proceedings of the 17th International Conference on Soil Mechanics and Geotechnical Engineering*, Alexandria, Egypt, October.
Zhou, M., Dang, F., Li, Y., Ding, J. and Gao, J. (2021), "Study on critical hydraulic gradient theory of flow soil failure in cohesive soil foundation", *Geofluids*, **2021**(1), 5599977. https://doi.org/10.1155/2021/5599977.

IC